UNIVERSITÀ DI PARMA

ARCHIVIO DELLA RICERCA

University of Parma Research Repository

Combined impact of B2H6 flow and growth temperature on morphological, structural, optical, and electrical properties of MOCVD-grown B(In)GaAs heterostructures designed for optoelectronics

This is the peer reviewd version of the followng article:

Original
Combined impact of B2H6 flow and growth temperature on morphological, structural, optical, and electrical properties of MOCVD-grown B(In)GaAs heterostructures designed for optoelectronics / Hidouri, T.; Parisini, A.; Ferrari, C.; Orsi, D.; Baraldi, A.; Vantaggio, S.; Nasr, S.; Bosio, A.; Pavesi, M.; Saidi, F.; Fornari, R.. - In: APPLIED SURFACE SCIENCE. - ISSN 0169-4332. - 577:(2022), p. 151884.151884. [10.1016/j.apsusc.2021.151884]

Availability:
This version is available at: 11381/2912788 since: 2022-01-20T10:45:02Z

Publisher:
Elsevier B.V.

Published
DOI:10.1016/j.apsusc.2021.151884

Terms of use:

Anyone can freely access the full text of works made available as "Open Access". Works made available

Publisher copyright

note finali coverpage

(Article begins on next page)

14 May 2024

Combined impact of B_2H_6 flow and growth temperature on morphological, structural, optical, and electrical properties of MOCVD-grown B(In)GaAs heterostructures designed for optoelectronics

Tarek Hidouri[*1,2], Antonella Parisini[1],

Claudio Ferrari[3], Davide Orsi[1], Andrea Baraldi[1], Salvatore Vantaggio[1], Samia Nasr[5,6], Alessio Bosio[1], Maura Pavesi[1], Faouzi Saidi[2], Roberto Fornari[1,3]

[1] University of Parma, Department of Mathematical, Physical and Computer Sciences, Viale delle Scienze 7/A 43124 Parma, Italy

[2]Micro-Optoelectronic and Nanostructures Laboratory, LR99ES29, Department of Physics, Faculty of Sciences Monastir, University of Monastir, Street of Environment, 5019 Monastir, Tunisia

[3]Institute of Materials for Electronics and Magnetism (IMEM-CNR), Viale delle Scienze 37/A, 43124, Parma, Italy

[5]) Advanced Functional Materials & Optoelectronic Laboratory (AFMOL), Department of Physics, Faculty of Science, King Khalid University, P.O. Box 9004, Abha, Saudi Arabia.

[6]) Electrochimie, Matériaux et Environnement (UREME [16ES02]), Institut préparatoire aux études d'ingénieurs Kairouan, Tunisia

*) Corresponding author: hidouritarek@gmail.com (Tarek Hidouri)

Abstract

BGaAs/GaAs epilayers and BInGaAs/GaAs quantum well (QW) have been prepared using metal-organic chemical vapor deposition under different growth conditions, and their physical and structural properties have been examined. SEM-EDS investigation showed a dependence of surface properties of the ternary compound on the growth conditions. High-resolution X-ray diffraction evidenced a tensile strain for the ternary alloys whatever the growth condition, while the quaternary QW always shows a compressive strain state. Room temperature optical absorption allowed to follow the variation of the bandgap with boron incorporation. Photoluminescence measurements confirmed the carrier-localization phenomenon and its dependence with the growth conditions. Deposition temperature and diborane (B_2H_6) flow rate are with particularly significant effects on the optical properties: lower diborane flow rate and high growth temperature enhance the radiative emission. Computer simulation using localized state ensemble model quantitatively relates the lattice inhomogeneity to the optical properties and suggests a way to engineer the localization phenomenon and avoid clustering effects. Electrical investigations by current-voltage, capacitance and conductance methods have

been performed for the first time on selected BGaAs samples. The ideality factor of Schottky barriers has been determined, while their height and film doping level could only be approximately estimated. Such physical properties make boron-based alloys very promising for applications in multijunction solar cells.

Keywords: B(In)GaAs; B_2H_6; growth temperature; localization; MOCVD; optoelectronics.

- **Introduction**

While many studies have been reported on the growth of BP and of $B_{12}P_2$ [1-3], the bibliography on BAs and $B_{12}As_2$ is much more limited. This is largely due to the difficulties encountered during their synthesis. These borides are wide gap semiconductors and are of technological interest in high temperature applications, because of their electrical and optical properties. They are also potentially very advantageous for use in a radioactive environment due to their ability to self-heal the damage caused by β radiation and convert it into electricity [4].

The insertion of a small percentage of boron in the ternary InGaAs appeared as another promising avenue for the development of novel optoelectronic devices [5-7]. Indeed, thanks to the small covalent radius of boron, the compressive stress induced by the insertion of indium into GaAs can be partially or totally compensated, depending on the type of device targeted [5]. For example, a material such as $In_{0.45}Ga_{0.55}As$ is theoretically adequate for the emission of radiation at 1.3 µm. But, for such indium contents, the lattice mismatch to GaAs substrate increases to more than 3.2%, which creates problems for industrial application. For InP substrates based heterostructures, i.e $In_{1-x}Al_xAs$/InP, the lattice mismatch is higher and varies between 2.4% to 4.2%. Regarding the influence of boron on the bandgap energy of the material, only limited effects are expected, lower than nitrogen, because theoretical and experimental studies suggest that the bowing parameter of BGaAs would be much less important than that of GaAsN [8]. Accordingly, due to the bandgap similarity between GaAs (1.42 eV) and BAs (1.42 -1.9 eV respectively) at room temperature (RT), the substitution of a few percent of boron to gallium in GaAs should not cause significant variations in the bandgap, contrarily to the very pronounced effects due to nitrogen. Thus, boron incorporation can provide an efficient strain compensation in InGaAs/GaAs heterostructures, while leaving the bandgap virtually unchanged. The introduction of boron should thus allow emission at a wavelength of 1.3 µm from BInGaAs / GaAs quantum wells (QWs), i.e. a correspondingly high indium content, without relaxation and dislocation formation. In addition, thicker BInGaAs layers may be tailored to have a desired lattice match to GaAs [9], with a potential application as active layer in high efficiency solar cells. For this last application, we would need to lower the bandgap to 1.25 eV or 1 eV.
Such a possible application of B-containing III-V materials has been demonstrated in multi-junction solar cells in a previous work [10]. By modulating the boron content in these alloys, several applications in light detection or emission [11] become possible. However, the B incorporation presents issues related to its solubility in the alloys, which is in turn related to growth conditions. In this work, we investigated the effect of two parameters:

diborane flow and epitaxial growth temperature. It will be shown that the simultaneous adjustment of these two conditions will allow for an optimized BInGaAs growth and, as a result, extend the range of potential application.

The paper is organized as follows: first, the deposition of the samples by MOCVD is described and then the effects of diborane flow and growth temperature on surface morphology are discussed. Further, the structural properties of the films as a function of growth conditions are studied by means of HR-XRD measurements, while the optical properties are investigated by absorption spectra at room temperature (RT) and by photoluminescence at low temperature and RT. The obtained data are explained by a model including carrier localization and their thermal redistribution. Finally, electrical measurements on Schottky diodes fabricated on BgaAs epitaxial layers provide a first estimate, of the background doping level of such layers.

- **Sample preparation and characterizations**

The samples studied in this work were prepared by MOCVD under atmospheric pressure, in a T-shape horizontal reactor on weakly doped silicon Si (n~3-4 10^{17} cm^{-3}) (001) GaAs substrates with misorientation of 1° towards [110]. Diborane (B_2H_6), triethylgallium (TEG), trimethylindium (TMI) and arsine (AsH_3) were used as boron, gallium, indium, and arsenic precursors, respectively. H_2 was used as carrier gas (18 L/min). The arsine AsH_3 flow rate was kept constant at 2.7 10^{-3} mol/min, with a maximal V/III ratio of 310 necessary for ensuring morphological quality and structural stability [12]. Different series of ternary samples were grown by varying the diborane flow rate from 2 to 7.5 sccm (at fixed high temperature of 580°C) ; correspondingly, The boron percentage in the gas phase, is varied from 30% to 69%, corresponds to the percentage of boron introduced in the gas phase relative to the total of elements III. This quantity is therefore defined as the ratio of the molar concentration of diborane to the total molar concentration of elements III. A factor of 2 is assigned to the diborane concentration because each mole of diborane provides 2 moles of boron:

$$x_v = {2[B_2H_6]}/{2[B_2H_6] + [TEG]}$$

A second series of BGaAs/GaAs was grown by varying the growth temperature in the range of 500°C to 600°C with a fixed high diborane flow of 7.5 sccm. The boron percentage in the gas phase is fixed at 62%. Combining the effects of the two growth parameters, tests were also made to prepare a quaternary BInGaAs/GaAs heterostructure. For the all BGaAs samples, the growth was performed for 60 minutes, giving an estimated film thickness between 150 nm and 200 nm. For the BInGaAs QW, the diborane, the trimethylindium (TMI) and the tryethylgallium (TEG) were used as precursors. The growth was performed at 580°C with a diborane flow of 2 sccm, a TMI and TEG flows of 2.8 10^{-6} mol/min and 4.2 10^{-6} mol/min respectively (used for the BGaAs). The arsine flow was keeped constant as for the BGaAs growth. The growth duration was fixed at 1 min which resulted in a thickness estimated to be 3-5 nm. The percentage of boron introduced in the gas phase for the quaternary is defined as :

$$x_v = {2[B_2H_6]}/{2[B_2H_6] + [TMI] + [TEG]}$$

Commentato [PA1]: Two verbs : I have eliminated « is »

The grown epilayers were analyzed with many characterization techniques. Scanning electron microscopy (SEM) experiments to investigate the surface morphology were performed using a Field-Emission SUPRA40 Zeiss SEM equipped with a GEMINI FESEM detection column (Zeiss, Germany). Energy Dispersive Spectroscopy (EDS) measurements were performed using a Silicon Drift Detector (SDD) X-act 10mm^2 LN2-free (Oxford Instruments) mounted on the SUPRA40 Zeiss SEM microscope. Samples were observed (5µm × 5µm) scale range by ex-situ atomic force microscopy with a Digital Instrument Nanoscope II in constant force mode (about 0.58 N/m). High-resolution X-ray diffraction (HRXRD) was performed using a High-resolution X-ray XPert-Pro diffractometer equipped with filtered CuKα radiation (1.540 Å). The diffractometer is provided with a Goebel mirror to increase the collected intensity from X-ray tube and a 4 reflection Ge 220 Bartel monochromator to reduce the beam divergence to 12 arcsec and beam dispersion $\Delta\lambda/\lambda$ to 10^{-4}. This removes any spurious peak that may arise from the non-perfect purity of x-ray source. Due to the very low size of the samples (<1 cm^2), they were mounted by a small droplet of a salt melting at low temperature. It is expected that this should not introduce spurious peaks to diffraction profiles. A focused ion beam equipped with an X-MaxN Energy Dispersive X-ray Spectroscopy (EDS) from Oxford Instruments, was used to perform EDS mapping of the surface of BGaAs heterostructures. The optical absorption spectra were measured at room temperature and normal incidence by using a Fourier transform infrared (FTIR) Bomem DA8 spectrometer over the 8500–12000 cm^{-1} range and resolution of 1 cm^{-1}. Steady state photoluminescence (PL) measurements were performed using the green line of the Continuous Wave (CW) Ar+ laser (514.5nm). PL measurements were carried out at cryogenic temperature (10 K) and by varying the power excitation and temperature (10K-300K). During temperature dependent PL measurements, samples were kept in a closed-cycle helium ~~circulation~~ cryostat. The emission is dispersed by a high-resolution spectrometer (Jobin-Yvon monochromator: focal length 0.6, resolution: 10 Å/mm width of the input slot, two 600 trait/mm diffraction gratings). Detection is done through a phototube with a built-in amplifier (up to ~ 10^4).

For electrical measurements, AuGe ohmic contacts were thermally evaporated on the sample surface and annealed at 400°C for 5 min. A matrix of Au Schottky contacts was realized on different layers by thermal evaporation or by sputtering of round dots (0.6 mm to 0.7 mm in diameter). The Au-dot pattern was annealed at 300 °C for 2 min. Before electrode depositions, the surfaces were refreshed by chemical etching (HCl for 1 min, rinsing in isopropyl alcohol and acetone). The Current-Voltage (I-V), the capacitance versus frequency (C-F) and the conductance versus frequency (G-F) measurements were performed to investigate different electrical characteristics of samples. A Sourcemeter Keithley Mod. 2400 and a HP 192A impedance analyzer were used for the electrical investigations. Theoretical calculations and modelling were performed using MATLAB software to solve the coupled equations and to explain the PL features as a function of temperature.

- **Results and discussion**

- **Effect of B_2H_6 flux ratio and growth temperature on the surface morphology of boron-based alloys**

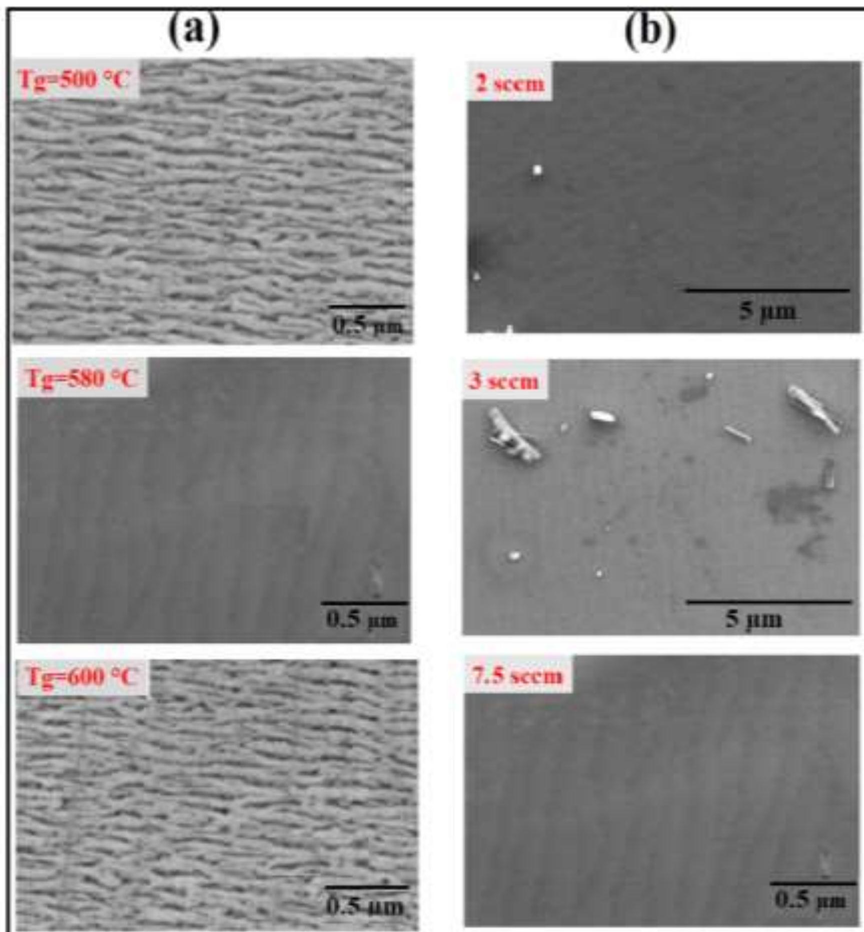

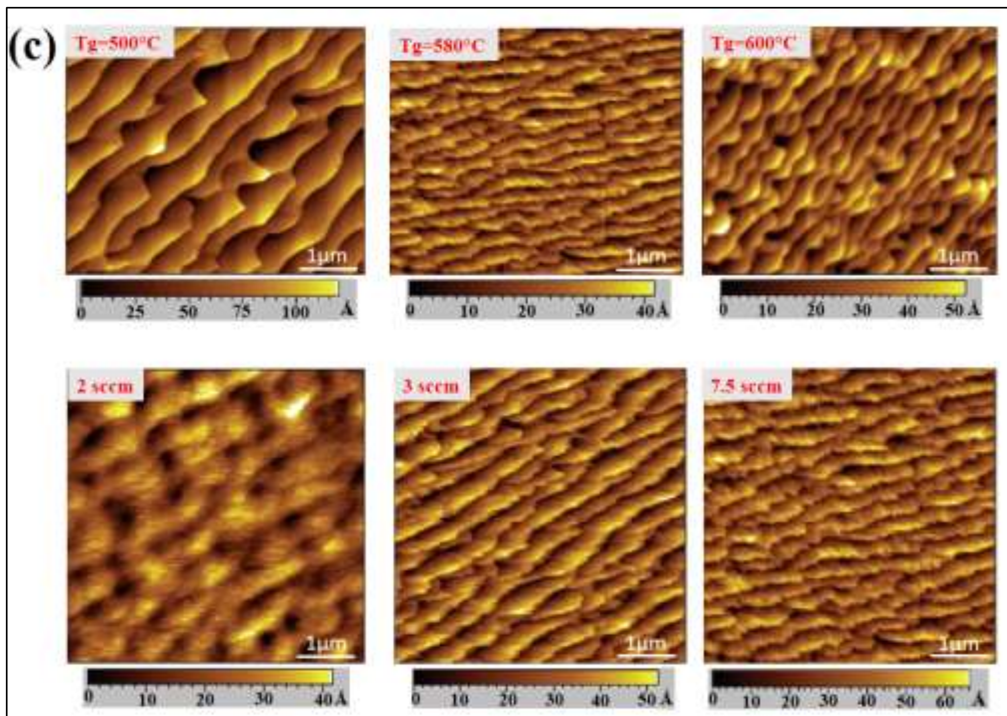
(c)
Tg=500°C
Tg=580°C
Tg=600°C
1μm
0 25 50 75 100 Å
0 10 20 30 40 Å
0 10 20 30 40 50 Å
2 sccm
3 sccm
7.5 sccm
0 10 20 30 40 Å
0 10 20 30 40 50 Å
0 10 20 30 40 50 60 Å

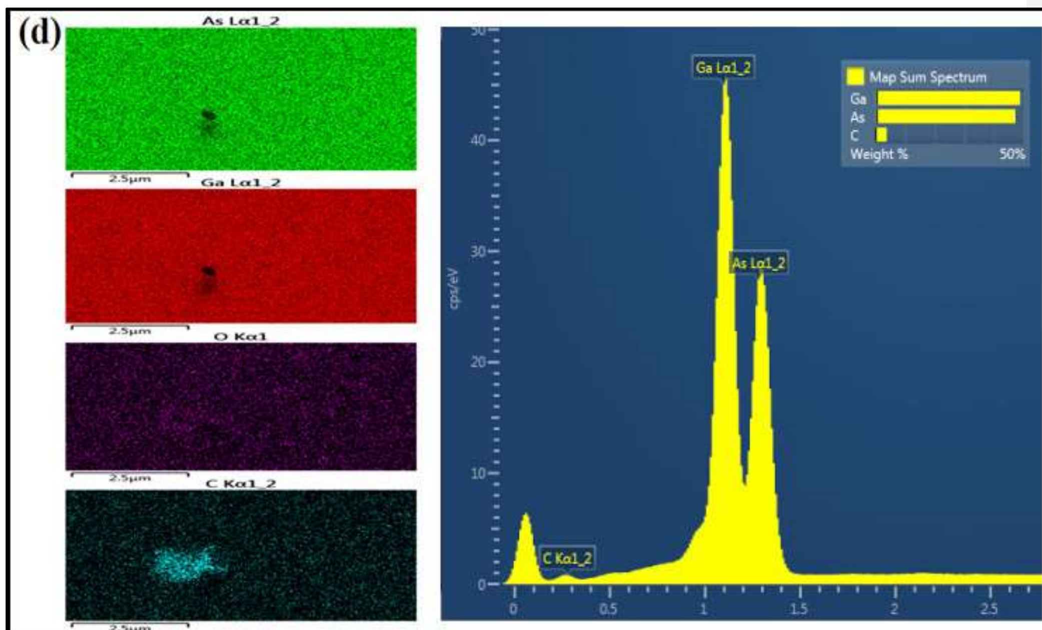
(d)
As Lα1_2
Ga Lα1_2
O Kα1
C Kα1_2
2.5μm
Ga Lα1_2
As Lα1_2
C Kα1_2
Map Sum Spectrum
Ga
As
C
Weight %
50%
cps/eV
0 0.5 1 1.5 2 2.5

Figure 1: (a) SEM image of BGaAs epilayers grown at different growth temperature: 500°C, 580°C and 600°C. (b) The effect of diborane flow rate: surface of samples grown with three different flow rates at 580°C are reported (at 7.5 sccm, the magnification has been changed for more clarity of the image). (c) corresponding AFM (5µm × 5µm) images of the same samples. (d) EDS mapping and integrated spectrum, highlighting the main film constituents and contaminants. The presence of Boron cannot be detected by the EDS equipment used, as discussed in the main text.

Figure 1a-b shows SEM images of the surface of samples deposited under different conditions and EDS maps of the dominant elements in the films. The growth temperature was increased from 500°C to 600°C (Figure 1a), keeping the B_2H_6 flow rate fixed at 7.5 sccm, and a high V/III flux ratio (V/III=310) to ensure system stability and to avoid the phase separation between the gallium-rich phase and the $B_{12}As_2$ phase. In fact, we have reported earlier that the growth at a low V/III flow rate leads to three-dimensional growth, high roughness, and a bad surface morphology [12]. By increasing the growth temperature at a fixed high diborane flow rate, step-bunching occurs, and steps and terraces appear. Also, diborane flow rate plays a role, as shown in Figure 1b, where the flux that increases from 3 to 7.5 sccm promotes the step-bunching. The impact of diborane flow on the surface morphology seems to be more significant than the growth temperature. At low flow rate (i.e 2 sccm), the 2D nucleation is confirmed (see Figure 1c). Width of terraces is much greater than the expected value (i.e 16 nm) for such a substrate's misorientation. In addition, the terraces are limited by steps of height multiple of 1 monolayer. These observations clearly confirm the occurrence of step-bunching. The increased diborane flow results in a marked widening of the terraces and a sharp increase of the steps' height i.e. a strong enhancement of step-bunching. AFM mapping illustrated in Figure 1c can confirm that the height of the steps increases from 2 to 10 monolayers by increasing the diborane flow at 580°C, while it passes from 12 to 27 monolayers at 500°C. The surface root mean square RMS has been found to be 23.3 Å, 8.5 Å and 13 Å, respectively by increasing the growth temperature from 500°C to 600°C. Meanwhile, upon increasin the diborane flow, the RMS increases 6.9 Å, 11.3 Å and 16.3 Å, respectively for samples grown with 2 sccm, 3 sccm, 7.5 sccm. Figure 1a-c clearly shows the strong dependence of terrace width and step height on deposition temperature and diborane flow rate. Furthermore, one can note that the distribution is also irregular, with regions where wide terraces coexist and other areas in which one can observe trains of steps very close to each other.

In the case of 2 sccm, the 2D nucleation on a vicinal surface reflects an insufficient diffusion length of adatoms to the front of the steps. The reduction of the diffusion length at 2 sccm is due to the fact that at very low flow rate of the III element precursor, the adsorbed species may find a suitable lattice site very rapidly and the residence time is very short, even if the desorption becomes improbable. Consequently the diffusion length decreases. On the other hand, in our present MOCVD conditions, step-bunching is associated to diffusion

lengths greater than the nominal width of the terraces. The transition of the growth mode suggests that the boron surface enrichment is accompanied by an increase of the surface mobility of Ga adatoms.

A previous X-ray photoelectron spectroscopic (XPS) study on BGaAs alloys proves a significant accumulation of B on the surface [10]. For this reason, we suggest that boron may act as surfactant and hence enhancing the surface mobility of gallium. The use of surfactants permits to modify the surface mobility of adatoms, their kinetics of attachment to the edges of steps, the surface energy, and its reconstruction, which indeed, can induce a change in the growth mode. Such behavior is similar to that observed when adding boron to GaAsN/GaAs [13], or the use of boron as surfactant in Ge/Si quantum dots [14, 15].

EDS measurements presented in Figure 1d indicate the presence of Ga, C, and As. The presence of carbon impurities is normal and originated from the residuals of of MOCVD precursors (Triethylgallium, TEG). However, we could not detect the presence of boron on the surface, because of the low system sensibility towards this very light element and of the limited amount of boron with respect to Ga and As (see Table 1). As boron is substituted to gallium in $B_xGa_{1-x}As$ matrix, the presence of boron can be followed accordingly to the gallium. The presence of boron can indirectly be inferred by step bunching and step meandering and from previous XPS measurements [10]. Indeed, we found that step bunching and meandering was accentuated under higher diborane flow rate. The meandering of the step front could be derived from the inhomogeneity of Ga diffusion rate, which is itself related to the inhomogenous distribution of boron on the terraces. The accumulation of boron at the steps can influence the incorporation kinetics of Ga in two ways: first, a higher boron content could increase the energy barriers for the Ga incorporation at the edge of the step from the upper terraces or lower ones. This effect could be a consequence of the substitution of B in Ga sites or to be linked to a change of the step structure (change of surface reconstruction). Second, the boron occupation at the edge of the steps may decrease the probability of Ga incorporation, and slow down the progression of the step fronts. Therefore, the inhomogeneous incorporation of boron may justify the observed step-bunching and variation of macrostep height. In the two cases, the signature of boron presence is shown.
For the quaternary BInGaAs/GaAs QW, deposited at 580°C under 2 sccm diborane flow, the step-bunching is again present (Figure 2c), even more pronounced, as evidenced by the widening of the terraces and an increase of the average height of steps (3-11 monolayers). However, the related morphology differs from that of the ternary BGaAs/GaAs grown in the same conditions with an RMS around 5 Å, and differs from the smooth reference layer of InGaAs/GaAs (see Figure 2a). The variation of surface morphology compared to the InGaAs is an indirect confirmation of the boron insertion (as explained before, the B element could not be detected by EDS). The B insertion is usualy accompanied by carbon incorporation due to the MOCVD conditions (Figure 2b). Such difference can be explained also by the higher surface mobility of indium adatoms compared to gallium adatoms [16] due to the boron’s presence on the surface. Another reason for the step-bunching could be the higher strain. In fact, *Tersoff et al.* [17] have proposed a model suggesting that the

strain could generate attractive long-distance interactions between the steps of a vicinal surface, leading to the leveling of these steps.

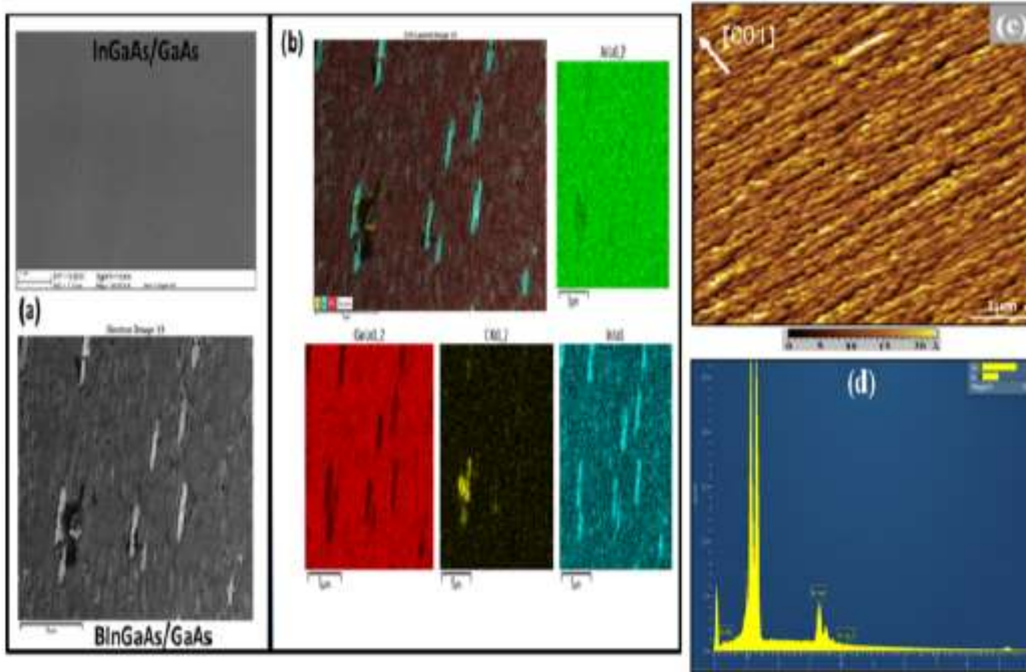

Figure 2: (a) SEM images of InGaAs/GaAs reference layer and of BInGaAs/GaAs QW grown at 580°C and 2sccm of diborane flow. (b) EDS elemental map of the QW surface showing the major In and Ga elements, (c) AFM (5µm × 5µm) image of the obtained QW, and (d) corresponding integrated EDS spectrum.

As suggested through the morphological properties, at high growth temperature, diborane flow is the most critical growth parameter as it determines the boron fraction in the compound, and determines the surface quality.

- **Structural analysis**

To investigate the effect of growth conditions on the structural properties and boron composition, HR-XRD measurements have been performed. Figure 3 shows the ω-2θ (004) scans of the B(In)GaAs samples measured in the vicinity of the GaAs (004) reflection. It is clear that the ternary alloys, whatever the growth conditions, are subject to a tensile strain. The fringes observed in all the samples corresponding to the lower mismatch demonstrate the vertical coherence of the substrate and epitaxial layers. Such fringes disappear in samples with higher mismatch due to the higher dislocation density introduces by the larger strain. Well-defined Pendellösung fringes have been generally observed in this type of samples [10, 12, 19] (elaborated by the

same reactor), which were demonstrating the vertical coherence of the substrate and epitaxial layers. These fringes are the result of the interference phenomenon due to the finite thickness of the layer. In the present samples, noise partially masks the fringes, quite visible in Figure 3a (sample of 3 sccm).

The GaAs peak is at 32° with respect to the 33° Bragg angle, because of the crystal miscut angle, however the BGaAs related peak is shifted to higher angle for increasing diborane flow. The same behavior is observed when we change the growth temperature. This shift is related to the higher boron concentration in the alloy. The full width at half maximum changes slightly by varying the diborane concentration. However, the effect seems larger with decreasing growth temperature, i.e. the growth temperature has more influence on the boron concentration than the diborane flow. It must also be noted that the incorporation of boron is limited at high temperature. The effect of limited incorporation of a given element at high temperature during epitaxy, well known for many compounds, is normally explained by surface desorption of the corresponding element.

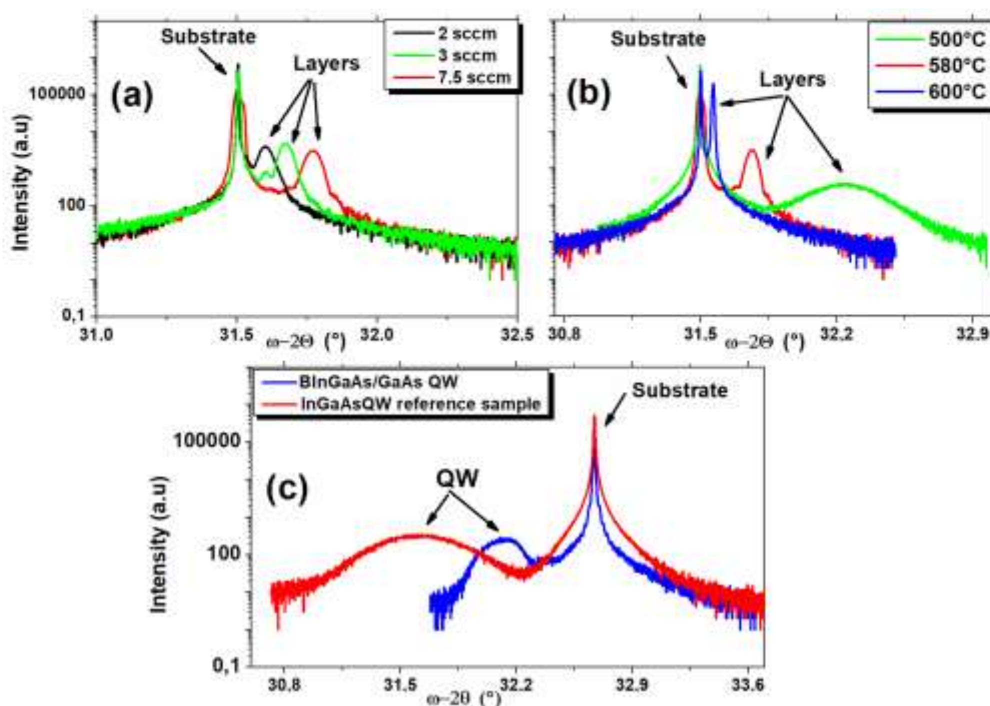

Figure 3: (004) ω-2θ scan of BGaAs/GaAs epilayers deposited with (a) different diborane flows and (b) different growth temperatures. (c) BInGaAs/GaAs related diffractogram compared to the InGaAs/GaAs reference sample.

This is the case, for instance, of low nitrogen incorporation in GaAs by MOVPE with dimethylhydrazine at temperature above 565 °C [18]. In the case of boron, the drop of boron incorporation at high growth temperature cannot be explained by the desorption at the growth interface, because at our growth temperatures the escape pressure of boron is too low. The hypothesis of the desorption of a borate species, derived from the decomposition of diborane, was considered and ruled out by *Geisz et al.* [6] who could not identify any boron species having an evaporation energy higher or even close to the activation energy of 4.1 eV (i.e energy for detaching a borate molecule).

To explain the drop of B incorporation in our layers, we must rather think of parasitic reactions in the gas phase. Indeed, such reactions are characterized by the formation of higher boranes i.e. boron hydrides B_xH_y, at high temperature, which are thermally more stable.

To evaluate the boron fraction and strain state, a combination of Bragg and Vegard laws has been used, supposing a total coherence in the structure. A more detailed calculation used for boron-based heterostructures can be found in Ref [19]. The calculated values have been reported in Table.1.

Table.1: Boron (x), indium (y) fractions and the calculated mismatch determined for every growth condition for ternary alloys and the derived quaternary QW.

Diborane flow rate @ 580°C		
2sccm	x=0.78%	$\Delta a/a$= -2.22 10^{-3}
3sccm	x=1.47%	$\Delta a/a$= -4.4 10^{-3}
7.5sccm	x=2.25%	$\Delta a/a$= -7.39 10^{-3}
Growth temperature @ B_2H_6=7.5 sccm		
500°C	x=6.54%	$\Delta a/a$= -19 10^{-3}
580°C	x=2.25%	$\Delta a/a$= -7.4 10^{-3}
600°C	x=1.5%	$\Delta a/a$= -1.72 10^{-3}
The obtained Quaternary BInGaAs @ 2sccm; 580°C		
InGaAs reference	y=17.8%	$\Delta a/a$= 8.46 10^{-3}
BInGaAs/GaAs	y=15%; x=2.1%	$\Delta a/a$= 3 10^{-3}

Whatever the boron composition, a negative lattice mismatch is determined for the ternary layers elaborated on GaAs. This B-induced tensile strain has a great effect, especially in compensating the compressive strain of InGaAs ternary on the GaAs. Note the large effect of 2 % of boron addition to the InGaAs in terms of reduction of lattice mismatch (about three times smaller). This is an encouraging result that extend the findings of a previous work [20] that showed how the low growth temperature is a key factor for the growth of BInGaAs/GaAs quaternary with a fraction of boron high enough to compensate the compressive strain. However, the low growth temperature and the high B content were seen to be coupled to a surface degradation

and poorer optical properties. In the present work, a quaternary alloy is grown at higher growth temperature with relatively low boron composition, while maintaining an effective strain compensation. Hence, the boron insertion is a good strategy for strain balancing, especially in compressively strained materials such as InGaAs/GaAs.

- **Optical study**

3a. Absorption investigations

Figure 4 shows the absorption coefficient (inset: Ln(α)) and Tauc plot, respectively, as function of photon energy for the BGaAs/GaAs layers grown at different diborane flows and growth temperatures.

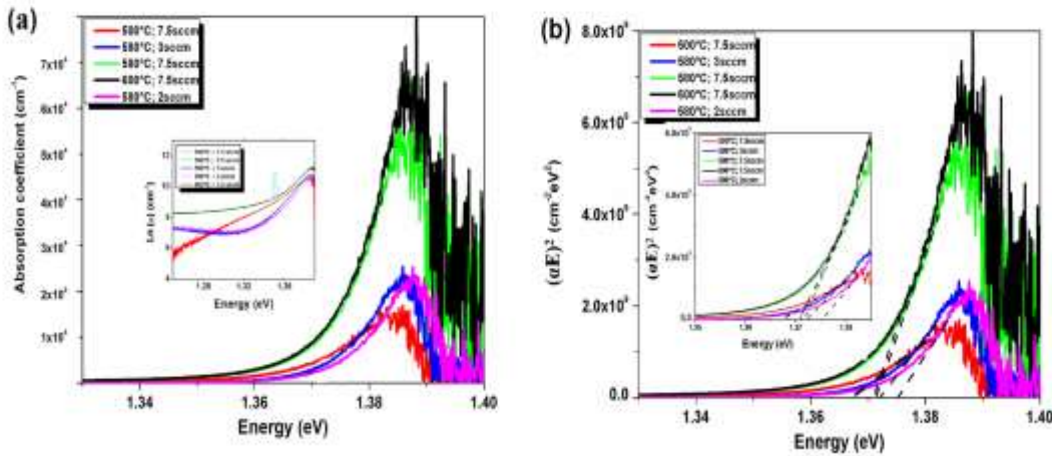

Figure 4: Room temperature optical absorption measurements performed on BGaAs/GaAs epilayers showing (a) the absorption coefficient (inset: Ln (α)) and (b) the Tauc plot versus photon energy for different growth conditions (inset : zooming on the determination of E_g from the Tauc plot (dashed black lines): no significant difference between samples prepared at 580 °C and 600°C for 7.5 sccm). The arrow in the inset of (a) indicates the linear part of the characteristics.

The layer grown at the highest growth temperature and diborane flow shows the highest absorption coefficient. In the inset of Figure 4a, the behavior of (ln (α)) versus the photon energy for lower growth temperature is quite linear (indicated by an arrow) before reaching the bandgap edge, indicating remarkable absorption processes involving states inside the bandgap. In heterostructures such as BGaN/AlN [21] this behavior was attributed to defect states introduced during the growth, because of the significant lattice mismatch between

buffer and layer at high boron fraction, giving rise to clustering and related deep electronic states. Such deep defect states in BGaAs layers have been detected and reported in a previous work [12].

The Tauc plots obtained from the absorption coefficient evolution are reported in Figure 4b. According to the Tauc law, $(\alpha E)^n = \beta(E-E_g)$, where α is the absorption coefficient and β is the slope of the curve, a linear trend is expected for the quantity $(\alpha E)^n$ when E is higher than the bandgap, with n=2 for a direct bandgap semiconductor. Note that by increasing the diborane flow, at a fixed high temperature, the band gap decreases. This behavior is anomalous compared to that usually observed in other conventional III-V alloys such as GaAlAs [22] and is consistent with a low value of the bandgap bowing parameter, in the range 2-4 eV, that explains the weak reduction of the bandgap of this material compared to the one of GaAs. For comparison, the GaAsN bowing parameter is much higher and extends between 16 and 20 eV depending on the nitrogen content [8]. At high growth temperature (580°C and 600°C) and a high diborane flow (7.5sccm) the absorption coefficient does not change while at lower growth temperature the bandgap results slightly higher (see inset Figure 4b).

The present results agree with the literature, see ref. [23, 24] and references therein, for lower boron fraction up to 2.5%, while for higher boron concentrations up to 7%, they agree with experimental results reported in [25, 26]. *Gottschalch et al.* [25] demonstrated that the PL emission energy of the $B_xGa_{1-x}As$ alloy shifts to higher energies for boron fractions greater than 1.2% while the intensity decreases. However, our results differ from those of *Ilahi et al.* [27] who reported a bandgap redshift for 8% boron fraction. This was ascribed to the formation of a continuous band tail which reduces the bandgap width and deteriorates the morphological quality of the surface [27].

3b. Photoluminescence investigations

Low temperature spectra

Figure 5 shows the PL spectra of the ternary and quaternary heterostructures recorded at 10K. The results do agree with the absorption measurements: the PL intensity decreases for increasing diborane flow, and then it tends to stabilize at high flow (see in Figure 5a the PL spectra as function of diborane flow). Note that it happens for all peaks, at lower (about 1.37 eV) and higher energy (about 1.47 eV). The GaAs substrate emission, expected in the range 1.45 -1.5 eV, is overlapped by contributions due to impurities introduced along with B during MOCVD deposition. The relatively broad band at 1.47 eV surely comes from the substrate but surprisingly its intensity changes with increasing B fraction in the layers. Probably this peak arises from contamination of GaAs during the deposition, in particular from the ($e\text{-}C_{As}$) transition related to carbon contamination and its optical LO-phonon replica, and the shallow Si-donor to C-acceptor recombination (the substrate is heavily Si-doped). Higher diborane flow leads to stronger incorporation of impurity-related non-radiative centers, thus PL intensity drops. These data should be compared to a previous work demonstrating that a variation of the boron content versus the III/V flow ratio is coupled to typical emissions from deep levels [12]. Deep level emissions are absent here whatever the deposition condition.

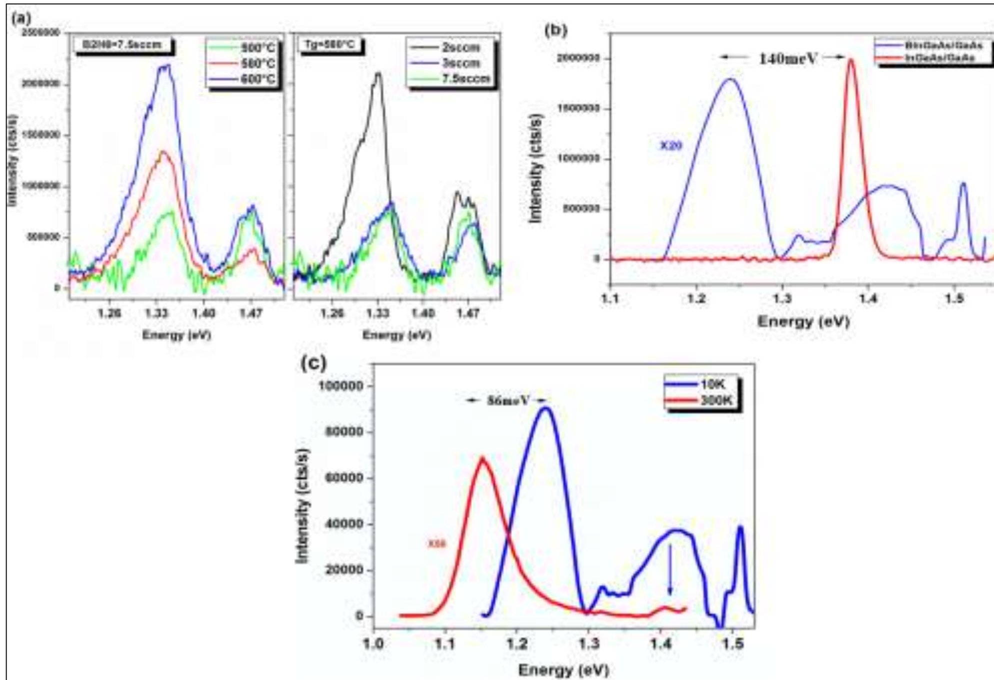

Figure 5: Low-T PL response of: (a) BGaAs/GaAs epilayers for different B_2H_6 flow rates and growth temperatures. (b) Low-T PL emission of the reached quaternary BInGaAs/GaAs QW compared to the InGaAs/GaAs reference sample and (c) the low-T PL spectrum of BInGaAs/GaAs QW compared to the room temperature emission.

A blue shift is clearly observed when increasing the diborane flow from 2 to 3 sccm, whereas passing from 3 sccm to 7.5 sccm there is no detectable shift. The initial shift is due to the enhanced strain related to the boron fraction, which is however much less effective at the highest flow due to the low bowing parameter of BGaAs alloys, and consequent milder bandgap variation at the highest B concentration. Consistent results are also obtained when looking at the PL behavior in samples grown at different temperatures. The sample grown at high diborane flow and high growth temperature is the most luminescent. The energy variation of the PL emission is not linear (no continuous blue/redshift), a result due to the interplay between the boron concentration and density of the non-radiative centers.

Whatever the growth condition, the PL emission is always broad and asymmetric, with a tail towards the low energy side. These asymmetries are characteristics of localized excitons related to boron clusters that may

give rise to discrete levels or bands below the conduction band. The formation of discrete levels or bands (that actually reduce the bandgap width) depends on the B concentration (i.e for a high cluster concentration a mini-band tends to be formed with consequent reduction of the bandgap). Such an asymmetric behavior is absent in the InGaAs/GaAs sample, which simply shows a fine symmetric emission blue-shifted towards higher energies, related to the compressive strain from indium alloying.

The quaternary alloys BInGaAs/GaAs has been grown at high growth temperature and low diborane flow rate (2 sccm). PL results obtained at 10 and 300 K are in the Figure 5c: the chosen QW (2 sccm; 580 °C) emits at 140 meV below the InGaAs and its emission persists up to room temperature (Figure 5b). Emissions around 1.5 eV are originated from the GaAs substrate and are influenced by (e-C_{As}) transitions related to carbon contamination and relevant LO-phonon replica. Two specific emissions are systematically observed for this BInGaAs/GaAs QW: a dominant RT emission peaked at about 1.24 eV and a secondary, less intense, at the higher energy side, which is due to an interfacial layer with lower indium content. This layer appears to be a common property for the quaternary QWs and has previously been observed by TEM [11], although its nature has not yet been explained. Actually, previous TEM analyses, carried out on $In_{0.2}Ga_{0.8}As$/GaAs quantum wells, produced in the same reactor, revealed abrupt interfaces [28], however we cannot rule out some indium segregation at the surface of the QW that ultimately could give rise to a thin "interfacial layer" of InGaAs during the deposition of the GaAs cap. The indium content gradually decreases by moving away from the well surface. This hypothesis is supported by the SEM images shown in the previous section, in which In accumulations on the surface is visible. Also, there could be a diffusion of In atoms towards the GaAs barrier. However, if this were the case, we should observe the same phenomenon between the QW and the GaAs buffer layer. But such effect was not observed.

We should note that the quaternary QW (2sccm; 580°C) chosen for this study shows the ~~lower~~ lowest energy emission with the highest intensity. This is an encouraging result in terms of optimization of these quantum wells. In particular, the emission energy shifts by 110 meV at RT and stabilizes at about 1.13eV (~1.1μm). This is a novel finding with respect to previous work on BInGaAs/GaAs QW deposited at lower growth temperature [11], and it proves that by extending the MOCVD growth window, including lower diborane flow and higher temperature, new types of QW becomes available, suitable for higher emission wavelengths.

Formattato: Evidenziato

Commentato [PA2]: ...shifts with respect to... ?

Formattato: Evidenziato

Formattato: Evidenziato

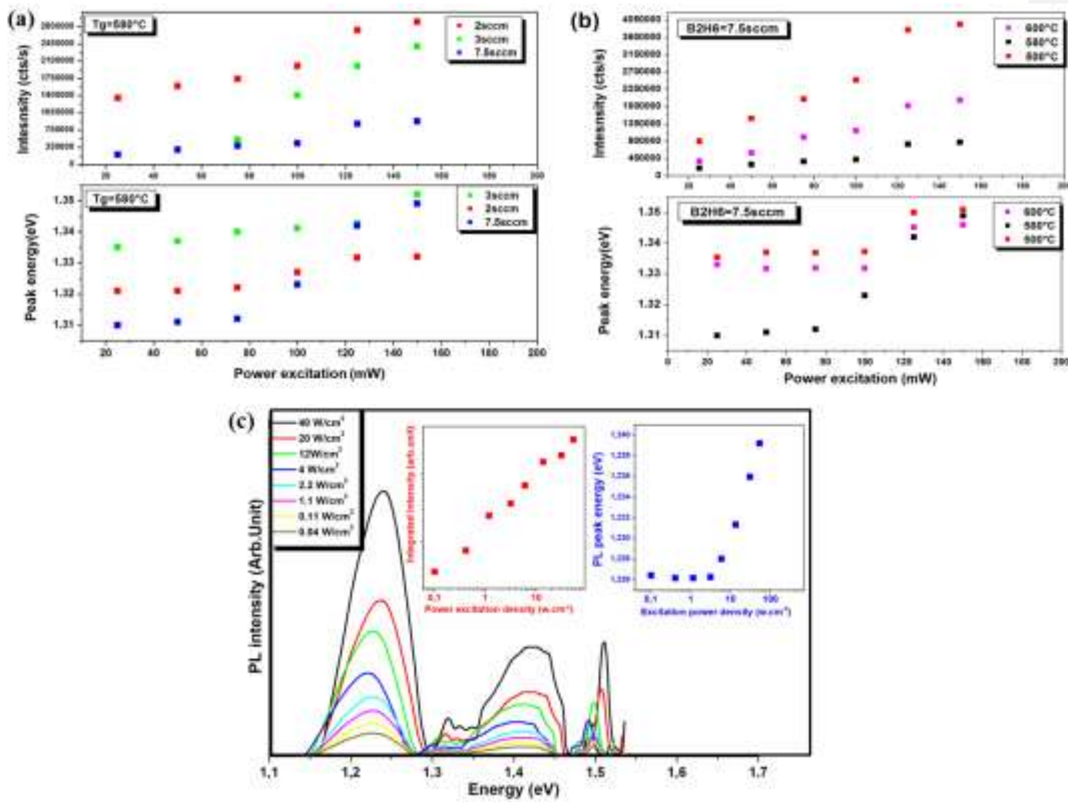

Figure 6: PL intensities and PL peak energy taken at different excitation power density on BGaAs/GaAs epilayers grown under two different (a) diborane flow rates and (b) different growth temperatures. (c) gives the PL emission versus photon energy for different excitation power on BInGaAs/GaAs QW grown at 580 °C with 2 sccm diborane flow. Insets : the PL intensity and the PL peak energy versus the excitation power density.

The spectra versus excitation power show that the main emission from the BGaAs/GaAs epilayers (deposited under different growth temperature and diborane flow) is around 1.33 eV and the asymmetry at low energy side persists whatever the excitation power. This means that such emission is intrinsic and characteristic of the investigated samples. In Figure 6a, we tested the PL peak position of the main emission as function of power excitation, which shows a blue shift. This is a signature on the progressive filling of higher energy states due to the increased density of photogenerated carriers. Two trends, dependent on the growth condition, are identified for the PL intensity (Figure 6a): a monotonic increase in the range 20-100 mW and a tendency to saturation, for excitation power higher than 120 mW. In any case, these behaviors are consistent with the presence of localization phenomena, which seems to strongly depend on the incorporated

boron fraction. The amplitude of the blue-shift and the saturation/no-saturation behavior can be related to the degree of potential fluctuations, intra-states redistribution, and carrier transfer in the band-tail. The lower the localization depth, the quickly the states are filled, showing a tendency toward an intensity saturation even at lower power excitation. This is well represented in Figure 6b for the sample deposited at 600°C (at 100 mW) and 500°C (at 125 mW), both with diborane flow of 7.5 sccm).

For the quaternary BInGaAs/GaAs deposited under 2sccm at 580°C, the PL intensity versus the incident power density tends to be linear (in log-log scale, see Figure 6c) and a sign of saturation begening appears between 12 W/cm^2 and 20 W/cm^2 ~~(showed by the blue arrow)~~, except a slight perturbation around 4 W/cm^2 (see inset in red color in figure 6c). However, this saturation is not complete as the PL intensity increases again in the last data point. This sign of saturation can be suported by the blue-shift observed in the PL peak energy versus the density of excitation (see blue inset in the same figure). The peak energy versus the density of excitation shows a sudden increase at a value around 12 W/cm^2 ~~(showed by the red arrow)~~. This is can be explained by the progressive filling of empty states with increasing the density of excitation. This supports the idea of localization phenomena also for the quaternary alloy. This will be confirmed in the next section.

Commentato [PA3]: The arrow was removed in the picture

Formattato: Evidenziato

Formattato: Barrato, Evidenziato

Formattato: Evidenziato

Commentato [PA4]: The arrow was removed in the picture

Formattato: Barrato, Evidenziato

Formattato: Evidenziato

3c. Photoluminescence study versus temperature

A systematic study of PL versus measurement temperature was performed to get more information about localization phenomena in ternary and quaternary compounds. Investigations were performed in the range 10-300 K on BGaAs/GaAs epilayers and the BInGaAs/GaAs QW with a fixed maximum power excitation of 150 mW.

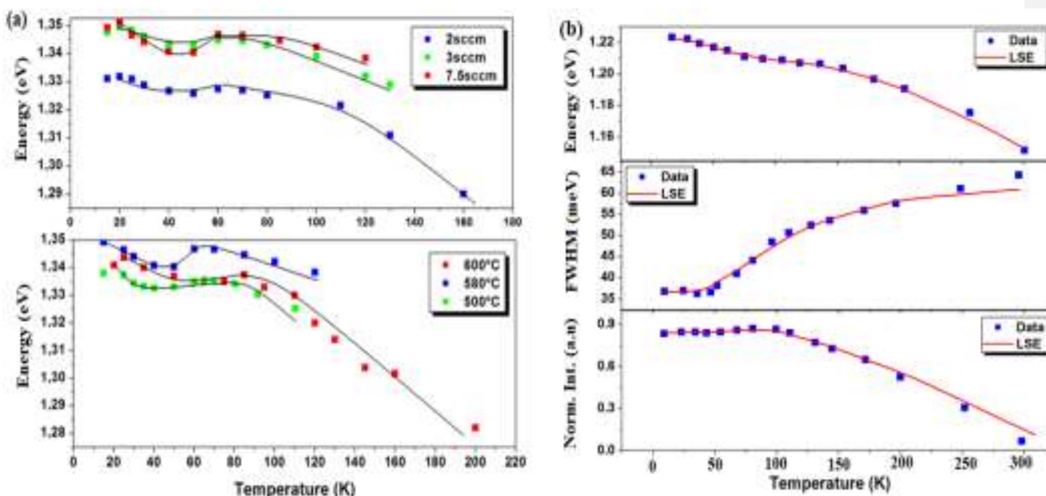

Figure 7: The PL peak position, the full width at half maximum and the normalized intensity versus the temperature for: (a) BGaAs/GaAs epilayers grown with different diborane flow rates and different growth temperatures. Data (colored squares) are fitted with the LSE model (black solid lines). (b) for the Quaternary

BInGaAs/GaAs QW deposited at 580°C and diborane flow of 2 sccm. Data (blue squares) are fitted by the LSE model (red solid lines)

Figure 7a-b reports the PL peak position, the full width at half maximum and the normalized intensity versus temperature for the BGaAs/GaAs epilayers and the BInGaAs/GaAs QW. For those alloys, independently of growth conditions, the PL response maintains the S-shaped form of the peak-energy dependence on T. This is a well-known mark of carrier localization phenomena, generally associated with the sub-bandgap potential fluctuations normally induced by strain, elemental composition inhomogeneity, defects, and interface roughness and/or fluctuation in the well width. The disorder can locally modify the valence and conduction bands by creating irregular fluctuations of the electrostatic potential. In boron-based alloys, due to the different ionic size and electronegativity between B and Ga, either isolated B atoms, B-B pairs and B clusters may introduce resonant defect levels, below the conduction band edge of BGaAs. As a result, at low temperature and low excitation density, excitons thermalize and relax to local minima where they get trapped. This phenomenon induces the first redshift observed for the PL peak energy. With further increase of T, carriers gain enough thermal energy to occupy higher energy states in the band-tail until they finally reach the conduction band edge. This process leads to a blue shift of the PL peak energy. Finally, for even higher temperature, carriers are thermally activated which prevents them from localization. Consequently, they can recombine freely, which in turns results in the second redshift of the PL peak energy.

We attributed the slight blue-shift at low temperature to the shallow states, most probably related to an anti-site, i.e. atom III replacing an atom V or vice-versa. A theoretical "full tight binding" calculation was performed by *Lindsay et al.* [29] to study the band structure. They used a BGaAs supercell with 2.06% of boron fraction, where 13 Ga atoms are replaced by B atoms. If boron atoms are considered isolated, a small blue shift is observed, which is apparently consistent with the present experimental results. The hypothesis of isolated B atoms is however weak and, most probably, B-B pairs or even boron clusters give the major contribution to PL emission shift.

From Figure 7a, the increased diborane flow rate enhances the localization linearly from 7 meV to 11.3 meV. The same trend is observed for the series of samples deposited at different temperature but fixed high diborane flow (7.5 sccm). This indicates that the B_2H_6 flow is the major generator of disorder and the principal controller of the localization. The PL intensity of the sample deposited with 2 sccm at 580°C persists at high ~~PL~~ temperature. For the two other samples of the same series the related luminescence drops faster. This confirms that the localization phenomenon significantly influences the optical response of the samples. Meanwhile, the presence of the localization is potentially accompanied by a high density of non-radiative centers and a faster thermal quenching. Same trend could be observed for the BGaAs/GaAs epilayer grown with 7.5 sccm at 600°C. We can say that the main localization generator in this kind of ternary compound could be the strain and/or composition fluctuations. Indeed, from XRD results, an enhanced tensile strain with decreasing the growth temperature, in parallel to the higher B fraction, was observed. Additionally, it resulted in a milder S-

shape profile indicating a *reduced effect of the compositional fluctuations*. In conclusion, the composition fluctuation remains the major disorder (i.e localization) generator. Such a phenomenon has been observed also in alloys such as GaAsSb.

It has been shown that higher growth temperatures result in *long-range ordering*. Atomic ordering generally induces a bandgap reduction [30]. This is the case for samples grown at 580°C and 600°C (except for 500°C-sample, in which the bandgap reduction is due to the formation of a continuous band-tail related to the higher boron incorporation rate). This suggests that the Group-V atoms in the sample grown at 500°C present a more random distribution compared to samples deposited at 580°C and 600°C, which would justify the slightly higher PL energy and the absence of the band-tail. We suggest that at higher growth temperature arsine and diborane may react to form very stable arsino-borane derivatives, thus making the gas phase poor of active boron species. It has been reported that the decomposition of diborane, at high temperature, leads to the formation of higher boranes (B_3H_9, B_4H_{10}…) [31], which ultimately reduces the concentration of active boron species supplied to the surface during growth and results in lower boron incorporation. On the other hand, lower growth temperature induces a random distribution of the Ga and B on the anion sublattice [32].

We performed a prototype growth of a quaternary BInGaAs/GaAs at 580°C, using a low diborane flow (2 sccm) to limit interactions between arsine and diborane in the gas phase, and to study the corresponding properties. The temperature-dependent PL features reported in Figure 7b show a marked drop of localization. The peak energy evolution shows an abrupt behavior compared to the quaternary deposited at 500°C studied earlier [20]. We attribute such a difference to a different degree of clustering. It seems that the density of states is lower for bigger clusters that tend to form a sub-band. The random clustering induces potential fluctuations and carrier trapping. However, trapped carriers are highly radiative and may thermally redistribute between clusters and give rise to a quasi-stable intensity in the range 10-80K. The interaction of carrier-phonon is low, which explains the reduction of the FWHM in the same temperature range. Thus, at higher temperature, carriers will move locally between clusters until they reach enough thermal energy to recombine classically, following the bandgap shrinkage. Carriers localized in the sub-band below the CB minimum are responsible for the absence of the blue-shift in the PL peak energy. The relatively high boron content tends to form a sub-band below the CB minima due to the increased density of clusters, which in turn reduces the potential fluctuations and disorder effects. This indicates that although present, the localization effects in quaternary alloys grown at higher growth temperature and low diborane flow are small and, even at low PL temperature, carriers have enough thermal energy to overcome the confinement potentials and get thermally transferred to higher energy states (i.e. in the band-tail and CB).

3d. Carrier redistribution model

A plot of the PL peak energy versus temperature provides useful information regarding the spatial distribution of carriers and its dependence on growth parameters. In an ideal system with no localization effects, the PL follows the temperature-dependent bandgap reduction described by the Varshni formula [33]

or the Bose-Einstein model as proposed by *Viña et al.* [34]. The Pässler model [35] is a five-parameter model that includes an additional empirical parameter 'p' related to the electron- phonon spectral function. This model will be used in this work to get a more accurate fitting of experimental data especially at low temperatures. The thermal redistribution quantity has been added to the empirical formula as follows:

$$E(T) = E(0) - \frac{\alpha\theta}{2}\left[\sqrt[p]{1+\left(\frac{2T}{\theta}\right)} - 1\right] - R(T)K_B T \qquad (1)$$

Here Θ and α are fitting parameters. R(T) is a temperature-dependent dimensionless parameter which can be obtained by numerically solving the following equation:

$$\left[\frac{1}{R}\left(\frac{\sigma}{K_B T}\right)^2 - 1\right] e^{-R} = \frac{\tau_r}{\tau_{tr}} e^{-(E_0 - E_a)/K_B T} \qquad (2)$$

τ_{tr} and τ_r are the time constant of thermal activation and radiative recombination respectively. E_0 and σ are the energetic center and width of the Gaussian-type density of states for localized-state ensemble distribution, respectively. K_B is the Boltzmann constant. A summary of the fitting parameters is presented in Table 2. The values for Θ and p were considered constant for the most part.

Table 2: Parameters used to fit the PL peak energy versus temperature for the investigated ternary BGaAs/GaAs and quaternary BInGaAs/GaAs samples

	E_a-E_0 (eV)	σ (eV)	α (eV/K)	Θ (K)	τ_r/τ_{tr}	p
Growth temperature						
500°C	0.005	0.0058	$6.4\ 10^{-4}$	240	20000	2
580°C	0.007	0.0094	$6\ 10^{-4}$	235	7500	2.3
600°C	0.01	0.0074	$6\ 10^{-4}$	231	3300	3
Diborane flow rate						
2sccm	0.01	0.007	$6.5\ 10^{-4}$	230	20000	2
3sccm	0.005	0.0082	$6\ 10^{-4}$	233	7500	2.3
7.5sccm	0.015	0.0113	$5.8\ 10^{-4}$	239	3300	3
Quaternary						
BInGaAs/GaAs		0.01	$6.8\ 10^{-4}$	430	6500	9

To correlate the PL properties of boron-based alloys with the compositional fluctuations following diborane flow and growth temperature variations, we shall consider all parameters reflecting the strength of localization phenomena, especially, σ, E_a-E_0, and related lifetime ratio.

It is apparent from experimental data that when the growth is performed under constant high diborane flow (varying the growth temperature), the carrier localization evolution is nonlinear. First, σ increases then it drops, because of the enhanced compositional inhomogeneity resulting from the increase of boron fraction at low growth temperature. The density of cluster-related electronic states will increase with increasing boron

incorporation until it reaches a quasi-saturation of the DOS (case of sample deposited at 500°C). States are much closer to each other, so facilitating the hopping process, and opening the possibility of reaching higher energy states. Indeed, even a low activation energy is enough to overcome the small barrier potentials, which explains the decrease of the magnitude E_a-E_0. This is not the case for samples grown at 580°C and 600°C for which states are less dense and remain well separated. As a result, higher activation energy is needed.

The calculations are made by considering a fixed radiative lifetime in the ratio between radiative and non-radiative lifetimes (τ_r/τ_{tr}). Indeed, the lifetime ratio increases with decreasing temperature, which corresponds to an increase of non-radiative rate (in the model, it is given by $1/\tau_{tr}$). This is normal as the boron insertion is accompanied by formation of non-radiative centers. Such an increase of the lifetime ratio is related to the E_a-E_0 magnitude. Higher activation energy means that states are more distant i.e. the density of states is lower. Consequently the probability of hopping between states is lower and, as a result, the probability of phonon-related recombination increases, which ultimately may increase the non-radiative transition lifetime.

For samples grown with different diborane flow rates, the localization depth increases linearly with the diborane flow. This indicates that, in those samples, the potential fluctuations follow the boron concentration corresponding to each diborane flow. Moreover, it seems that this growth condition affects the bandgap disorder more heavily than the growth temperature. Therefore, the expected localizations depths are larger by varying the B_2H_6 flow, although comparable for quaternary and ternary alloys. This means that the disorder inside the materials does not increases much even at the MOCVD-grown quaternary limits (high growth temperature). However, the magnitude E_a-E_0 is negative. This means that the local activation energy related to the localized states is below the band-tail center.

3e. Electrical investigation

Electrical investigation was performed for the first time on selected BGaAs samples to obtain information on their background doping level. The net Si-doping level of the substrate was about 10^{18} cm^{-3}. Schottky barriers were prepared on the top surface of the structure, and their quality was tested by current-voltage characteristics: an example is reported in Figure 8.

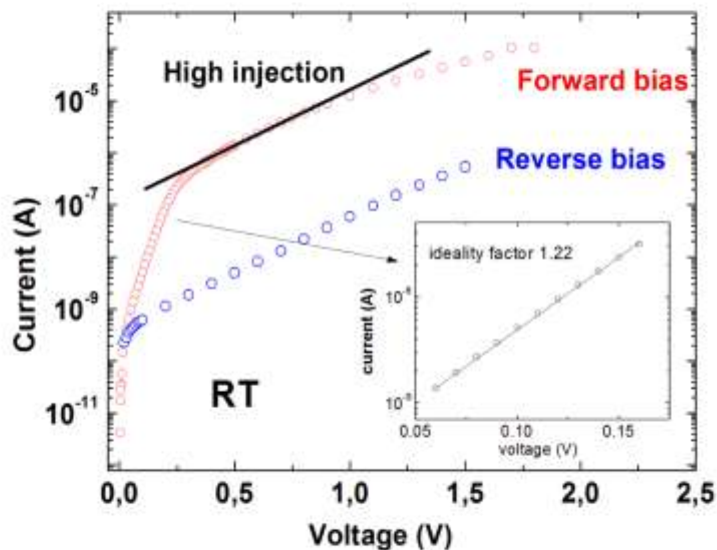

Figure 8: Current-voltage characteristic of Schottky barriers at room temperature. In the low-injection low-voltage region: an ideality factor of 1.22 is obtained. The high-injection region starts at a forward bias greater than about 0.3 V.

The low-injection region (low forward bias) shows an ideality factor of 1.22. This value is greater than the unity indicating that recombination through in-gap centers also contributes to current flow in addition to thermionic emission. Compared to $GaAs_{1-x}N_x$/GaAs layers doped Si, this value is greater than results founded by *W. Bouiadjra et al.* [36], in which the ideality factor is ranging between 1.04 and 1.16 respectively for a nitrogen content from 0.2% to 1.2%. Among the effects that must be considered to explain the relatively high ideality factor are the interface states, tunneling, non-uniformity distribution of the interfacial charges, electron traps in the semiconductor band gap (defect states), inhomogeneity of Schottky barrier height and generation-recombination currents within the depletion region.

The high-injection region appears at a forward bias of about 0.3 V: the linear trend in semilog-scale is consistent with a tunneling transport though the Schottky barrier (see Figure 8). Therefore, the knee at 0.3 eV just provides an underestimate of the barrier height, which is in reality higher. The mechanisms of transport across the junction and the rectification efficiency of the diode are expected to be influenced by the surface morphology, i.e. the growth conditions of the layer and amount of incorporated boron. The photo response to white light of the electrical characteristics was also recorded (see Figure 9).

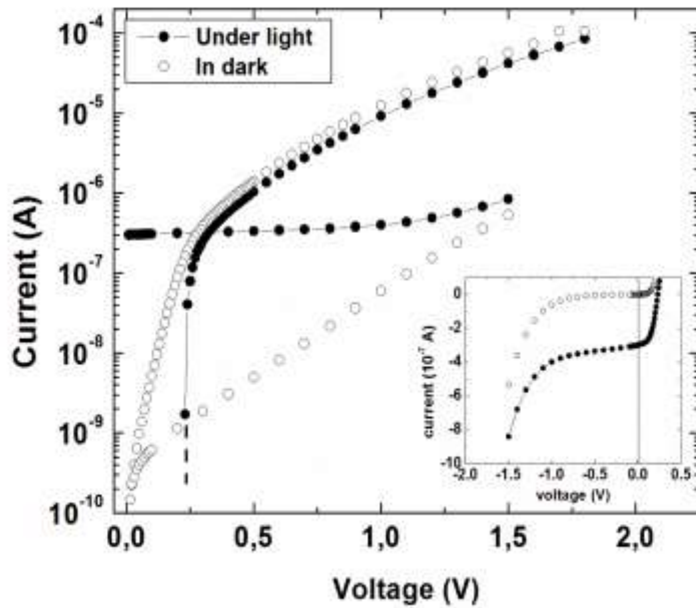

Figure 9: Current-voltage characteristic at room temperature under visible light: a weak photovoltaic effect is detected.

Despite the low barrier height, admittance spectroscopy measurements under external bias were possible. The capacitance measured on the same diode of Figure 8 showed very little variation with the reverse bias and with frequency in the range 10^2-10^6 Hz (see Figure 10a), as expected for a fully depleted layer with a space charge region extending over the entire layer thickness. Even under a forward polarization, no appreciable reduction of the depleted thickness was detected, as it was masked by effects of carrier injection already at a bias of a few tenths of V. Unfortunately, the complete film depletion did not allow using capacitance transient spectroscopy for detection and study of possible deep states.

Indeed, a depleted depth W=0.12 µm was calculated from the following relation :

$$C/_A = \varepsilon/_W \quad (3)$$

Where C is the capacitance, A is the area and, W is the depleted region thickness and, ε is the dielectric constant, taking the average experimental value C=3.8×10^{-10} F, a static dielectric constant $\varepsilon = 12.9\varepsilon_o$, with ε_o vacuum permittivity (slightly lower than GaAs), and a diode area A=3.85×10^{-7} m^2.

The thickness W of the depleted region is effectively comparable to the layer thickness. A critical analysis of PL investigations, strongly suggests that there is a negligible density of traps in our ternary and quaternary films. The net doping level $(N_D - N_A)$ can therefore be derived from:

$$W = \sqrt{\frac{2\varepsilon\phi_B}{e(N_D - N_A)}} \quad (4)$$

Considering a value of ϕ_B=0.3eV, reasonable for the Schottky barrier height although underestimated, a $(N_D - N_A)$ value of 3.2×10^{16} cm^{-3} is obtained for the residual impurity density. The conductance resulted of few 10^{-7} S, and weakly (sub-linearly) dependent on frequency (see Figure 10b). A static resistivity of about 10^{8} Ωcm was estimated, by neglecting the contributions due to contact and substrate series resistances and considering the area and the length of the transport channel equal to A and W reported above, respectively. This value is comparable to the intrinsic resistivity value of GaAs, consistently with the hypothesis of a fully depleted layer. Indeed, no effect of the boron on the intrinsic resistivity of boron-based ternary alloys was detected in this work. The data were reproducible, as proved by the results obtained for another diode having area 2.83×10^{-7} m^2.

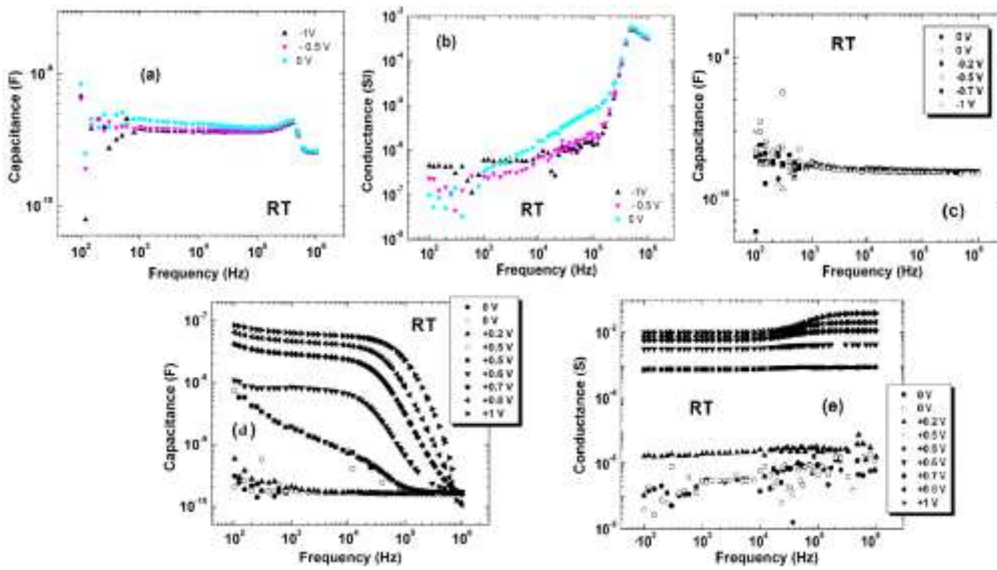

Figure 10: The capacitance (a) and the conductance (b) versus the frequency at room temperature (RT) for reverse bias values in diode 1. The RT capacitance (c) versus the frequency at RT for reverse bias values in diode 2. The RT capacitance (d) and the conductance (e) versus frequency at RT for forward bias values in diode 2.

The thickness of the depleted region and the calculated residual doping are actually in agreement also for the second diode, as demonstrated by the data reported in Figure 10 c-e, i.e. capacitance data versus the frequency under reverse bias, capacitance and conductance data versus frequency at forward bias (similar results were obtained also for the first one). Notice that both C and G increase with the increasing external polarization. At low frequency, the condition $C=G\tau_p$ is satisfied, with a relaxation time τ_p of a few 10^5 sec: for this reason, such a behavior has been reasonably attributed to carrier injection [37].

The global self-consistency of these results corroborates the hypothesis of low density of deep levels also suggested by PL investigation.

Conclusion

Morphological, structural, and optical properties of ternary BGaAs/GaAs epilayers grown at different growth temperatures and diborane flow rates were investigated. The surface morphology was seen to change from step-flow to step-bunching for increasing growth temperature and diborane flow. The light absorption and emission properties strongly depend on the boron incorporation related to the growth condition. Evidence of tensile strain was found in the analyzed epilayers.

The PL performances of the ternary heterostructures (BGaAs) and a QW structure (BInGaAs) were clearly dependent on carrier localization phenomena. Carrier localization is a crucial factor that can be tuned by changing the growth conditions and especially the diborane flow rate.

The PL spectra versus the temperature were fitted using the LSE model: a decrease of the PL peak width for low growth temperature and fixed high diborane flow was interpreted in terms of DOS saturation and formation of a mini band below the conduction band. However, the peak width was seen to increase with the B_2H_6 flow. Indeed, this flow rate appears as the factor that mostly influences the disorder inside ternary alloys.

The quaternary BInGaAs/GaAs was prepared following the optimized conditions for the ternary alloys. The obtained QW emits around 1.15eV at room temperature with a red shift of 140 meV compared to the simple InGaAs/GaAs QW. Such a result makes the MOCVD growth of boron-containing quaternary possible under special conditions and paves the way to novel applications in multi-junction solar cells.

The modeling of PL data of the quaternary layer shows a slight increase of the localization depth compared to the ternary InGaAs boron-free alloy grown in the same condition. Compared to the ternary BGaAs film deposited under a higher diborane flow rate, the decrease of localization depth in the BInGaAs quaternary is instead net. Assuming a constant radiative lifetime, the carrier lifetime ratio τ_r/τ_{tr} decreases considerably with B content, which implies an increase of the thermal quenching of luminescence and a decrease of carrier transfer time.

Measurements of Current-Voltage, capacitance, and conductance versus the frequency were performed for the first time on Schottky diodes fabricated on selected BGaAs samples. An ideality factor of 1.22 was obtained in the low injection region, and a capacitance of (3.5- 4.5) $\times 10^{-10}$ F with a dielectric constant of 12.9 ε_0. ~~For~~ Assuming a barrier height of 0.3 V, a background doping level of 3.2×10^{16} was estimated. Even at RT the

Formattato: Evidenziato

Schottky barrier on the ternary film exhibited a weak photovoltaic effect under visible light. Optical measurements did not detect any appreciable density of deep levels and electrical investigation supported this evidence.
In conclusion, this work shows that MOCVD is suitable for growing B-containing alloys and that by tailoring the deposition and diborane flow one can control the carrier localization phenomena, i.e. tune the optical properties. This is promising in view of future application of these ternary and quaternary films in photovoltaic applications.

Acknowledgements

The authors extend their appreciation to the Deanship of Scientific Research at King Khalid University for funding this work through research group program under Grant Number RGP. 2/203/42.

The stay of Dr. T. Hidouri at the University of Parma was made possible by Italian Ministry of Foreign Affairs and International Cooperation (MAECI).

References

[1] K. Shohno, M. Takigawa et T. Nakada, Epitaxial growth of BP compounds on Si substrates using the B2H6-PH3-H2 system, *J. Cryst. Growth.* **24-25** (1974) 193-196.

[2] G.A. Slack, T.F. McNelly et E.A. Taft, Melt growth and properties of B6P crystals, *J PHYS CHEM SOLIDS* **44** (1983) 1009-1013.

[3] Y. Kumashiro, Refractory semiconductor of boron phosphide, *J.Mater Research* **5** (1990) 2933-2947.

[4] T.L. Aselage et D. Emin, Brevet US n° : 6, 479,919. 12 novembre 2002.

[5] Radhia Hamila, Faouzi Saidi, Hassen Maaref, Philippe Rodriguez, and Laurent Auvray, Photoluminescence properties and high resolution x-ray diffraction investigation of BInGaAs/GaAs grown by the metalorganic vapour phase epitaxy method, *Int. J. Appl. Phys.* **112** (2012) 063109.

[6] J.F. Geisz, D.J. Friedman, S.R. Kurtz, J.M. Olson, A.B. Swartzlander, R.C. Reedy, A.G. Norman, Epitaxial growth of BGaAs and BGaInAs by MOCVD, *J. Cryst. Growth* **225** (2001) 372.

[7] HERBERT S. MĄCZKO, ROBERT KUDRAWIEC, AND MARTA GLADYSIEWICZ, Optical gain sensitivity of BGaAs/GaP quantum wells to admixtures of group III and V atoms Opt. Mater. Express **10** (2020) 2962.

[8] U. Tisch, E. Finkman, *and* J. Salzman, The anomalous bandgap bowing in GaAsN *Appl. Phys. Lett*. **81** (2002) 463.

[9] Z. Jia, Q. Wang, X. Ren, Y. Yan, S. Cai, X. Zhang, Y. Huang, and X. Duan, Asia Communications and Photonics Conference, OSA Technical Digest (online) (Optical Society of America, 2012), paper AS1H.3.

[10] Tarek Hidouri, Mahitosh Biswas, Indranil Mal, Samia Nasr, Subhananda Chakrabartie, Dip Prakash Samajdar, Faouzi Saidi Engineering of carrier localization in BGaAs SQW for novel intermediate band solar cells: Thermal annealing effect *Sol Energy* **199** (2020) 183-191.

[11] Tarek Hidouri, Radhia Hamila, Ibtissem Fraj, Faouzi Saidi, Hassen Maaref, Philippe Rodriguez, Laurent Auvray, Investigation of the localization phenomenon in quaternary BInGaAs/GaAs for optoelectronic applications *SUPERLATTICE MICROST.* **103** (2017) 386-394.

[12] Tarek Hidouri, Faouzi Said, Hassen Maaref, Philippe Rodriguez, Laurent Auvray, Impact of photoluminescence temperature and growth parameter on the exciton localized in BXGa1-XAs/GaAs epilayers grown by MOCVD *Opt. Mater.* **60** (2016) 487-494.

[13] F. Dimroth, A. Howard, J.K. Shurtleff et G.B. Stringfellow, Influence of Sb, Bi, Tl, and B on the incorporation of N in GaAs *J. Appl. Phys* **91** (2002) 3687-3692.

[14] H. Takayima, M. Miura, N. Usami, T. Hattori et Y. Shiraki, Drastic modification of the growth mode of Ge quantum dots on Si by using boron adlayer *Thin Solid Films* **369** (2000) 84-87.

[15] P.S. Chen, Z. Pei, Y.H. Peng, S.W. Lee et M.J. Tsai, Boron mediation on the growth of Ge quantum dots on Si (100) by ultra-high vacuum chemical vapor deposition system *Mater. Sci. Eng., B* **108** (2004) 213-218.

[16] A. Palma, E. Semprini, A. Talamo et N. Tomassini, Diffusion constant of ga, in and as adatoms on gaas (001) surface: molecular dynamics calculations *Mater. Sci. Eng., B* **37** (1996) 135-138.

[17] J. Tersoff; Y.H. Phang, Z. Zhang et M.G. Lagally, Step-Bunching Instability of Vicinal Surfaces under Stress *PRL* **75** (1995) 2730-2733.

[18] L. Auvray, H. Dumont, J. Dazord, Y. Monteil, J. Bouix, C. Bru-Chevallier et L. Grenouillet, MOVPE growth of GaAsN : surface study by AFM and optical properties *MAT SCI SEMICON PROC* **3** (2000) 505-509.

[19] Tarek Hidouri, Samia Nasr, Indranil Mal, D.P. Samajdar, Faouzi Saidi, Radhi Hamila, Hassen Maaref, BGaAs strain compensation layer in novel BGaAs/InGaAs/BGaAs heterostructure: Exceptional tunability *Appl. Surf. Sci.* **524** (2020) 146573.

[20] T.Hidouri, F. Saidi, H. Maaref, Ph.Rodriguez, L.Auvray, LSE investigation of the thermal effect on band gap energy and thermodynamic parameters of BInGaAs/GaAs Single Quantum Well *Opt. Mater.* **62** (2016) 267-272.

[21] E. Zdanowicz, D. Iida, L. Pawlaczyk, J. Serafinczuk, R. Szukiewicz, R. Kudrawiec, D. Hommel, and K. Ohkawa, Boron influence on bandgap and photoluminescence in BGaN grown on AlN *J. Appl. Phys*. **127** (2020) 165703.

[22] M. E. Groenert, R. Averbeck, W. Hösler, M. Schuster, H. Riechert, Optimized growth of BGaAs by molecular beam epitaxy *J. Cryst. Growth* **264** (2004) 123-127.

[23] V.K. Gupta, M.W. Koch, N.J. Watkins, Y. Gao et G.W. Wicks, Molecular beam epitaxial growth of BGaAs ternary compounds *J. Electron. Mater.* 29 (2000) 1387-1391.

[24] Gus L. W. Hart and Alex Zunger, Electronic structure of BAs and boride III-V alloys *Phys. Rev. B* **62** (2000) 13522.

[25] V. Gottschalch, G. Leibiger, and G. Benndorf, MOVPE growth of BxGa1−xAs, BxGa1−x−yInyAs, and BxAl1−xAs alloys on (0 0 1) GaAs *J. Cryst. Growth* **248** 468-473 (2003).

[26] F. Saidi, R. Hamila, H. Maaref, Ph Rodriguez, L. Auvray and Y. Monteil, Structural and optical study of BxInyGa1− x− yAs/GaAs and InyGa1− yAs/GaAs QW's grown by MOCVD *J. Alloys Compd*. **491** 45-48 (2010).

[27] S. Ilahi, F.Saidi, R.Hamila, N.Yacoubi, H.Maaref, L.Auvray, Shift of the gap energy and thermal conductivity in BGaAs/GaAs alloys, *Physica B Condens* **421** (2013) 105–109.

[28] H. Choujaa, EPVOM et caractérisation d'alliages ternaires InGaAs – BGaAs. Application : Télécommunications à 1,3–1,55 µm, Rapport de DEA de l'Université Claude Bernard –Lyon 1, (2003).

[29] A. Lindsay, E. P. O'reilly, Theory of conduction band dispersion in dilute BxGa1−xAs alloys

Phys. Rev. B. **76** (2007) 075210.

[30] B. P. Gorman, A. G. Norman, R. Lukic-Zrnic, C. L. Littler, H. R. Moutinho, T. D. Golding, and A. G. Birdwell, Atomic ordering-induced band gap reductions in GaAsSb epilayers grown by molecular beam epitaxy *J. Appl. Phys*., **97** (2005) 063701.

[31] H. Fernandez, J. Grotewold and C.M. Previtali, Thermal decomposition of diborane. Part I. The decomposition mechanism at low conversion and temperature and the inhibiting effect of accumulated hydrogen *J. Chem. Soc., Dalton Trans.* **20** (1973) 2090-2095.

[32] Y. Kawamura, A. Gomyo, T. Suzuki, T. Higashino, N. Inoue, Band-gap change in ordered/disordered GaSb1-ySby layers grown on (0 0 1) and (1 1 1)B InP substrates, Jpn. *J. Appl. Phys.* **41** (2002) L447–L449.

[33] Y. P. Varshni, Temperature Dependence of the Energy Gap in Semiconductors, *Physica*, **34** (1967)149–154.

[34] L. Vina, S. Logothetidis, and M. Cardona, Temperature dependence of the dielectric function of germanium *Phys. Rev. B* **30** (1984) 1979-1991.

[35] R. Pässler, Basic Model Relations for Temperature Dependencies of Fundamental Energy Gaps in Semiconductors, *Phys Stat Sol B* **200** (1997) 155-172.

[36] Wadi Bachir Bouiadjra, Abdelkader Saidane, Abdelkader Mostefa, Mohamed Henini, M. Shafi, Effect of nitrogen incorporation on electrical properties of Ti/Au/GaAsN Schottky diodes SUPERLATTICE MICROST **71** (2014) 225–237.

[37] S. Duman, B. Gürbulak, S. Do_gan, A. Türüt, Capacitance and conductance–frequency characteristics of Au–Sb/p-GaSe: Gd Schottky barrier diode Vacuum **85** (2011) 798-801.